

## Research Article

# Atorvastatin Inhibits Ferroptosis of H9C2 Cells by regulating SMAD7/Hepcidin Expression to Improve Ischemia-Reperfusion Injury

You Peng,<sup>1,2,3</sup> Bin Liao,<sup>2</sup> Yan Zhou,<sup>2</sup> Wei Zeng,<sup>2</sup> and Zhi-Yu Zeng<sup>1</sup> 

<sup>1</sup>Department of Geriatric Cardiology & Guangxi Key Laboratory of Precision Medicine in Cardio-Cerebrovascular Diseases Control and Prevention & Guangxi Clinical Research Center for Cardio-Cerebrovascular Diseases, The First Affiliated Hospital of Guangxi Medical University, Nanning, Guangxi, China

<sup>2</sup>Department of Geriatric, Hunan Provincial People's Hospital, The First Affiliated Hospital of Hunan Normal University, Changsha, Hunan, China

<sup>3</sup>Hunan Research Institute of Geriatrics, Changsha, Hunan, China

Correspondence should be addressed to Zhi-Yu Zeng; zengzhiyu@gxmu.edu.cn

Received 14 July 2022; Accepted 27 October 2022; Published 8 November 2022

Academic Editor: Stefan Simovic

Copyright © 2022 You Peng et al. This is an open access article distributed under the Creative Commons Attribution License, which permits unrestricted use, distribution, and reproduction in any medium, provided the original work is properly cited.

**Background.** Ferroptosis plays a key role in cardiomyopathy. Atorvastatin (ATV) has a protective effect on ischemia-reperfusion (I/R) cardiomyopathy. The purpose of this study is to elucidate the mechanism of ATV in I/R injury. **Methods.** H9C2 cells and cardiomyopathy rats were induced by hypoxia/reoxygenation (H/R) and I/R to construct *in vitro* and *in vivo* models. Cell viability was determined by CCK8. Cardiac histopathology was observed by HE staining. Transmission electron microscope (TEM) was used to observe the mitochondrial morphology. The reactive oxygen species (ROS) content in cells was analyzed by the biochemical method. ELISA was conducted to calculate the concentrations of total iron/Fe<sup>2+</sup> and hepcidin. The expression of ferroptosis and SMAD pathway-related genes were detected by qPCR. Western blot was performed to detect the expression levels of ferroptosis and SMAD pathway-related proteins. **Results.** In H9C2 cells, ATV reversed the decline in cell viability, mitochondrial shrinkage, and ROS elevation induced by erastin or H/R. The concentration of total iron and Fe<sup>2+</sup> in H/R-induced H9C2 cells increased, and the protein expression of FPN1 decreased. After ATV treatment, the concentration of total iron and Fe<sup>2+</sup> decreased, and the protein expression of FPN1 increased. The expression of the SMAD7 gene in H/R-induced H9C2 cells decreased, and the expression of the hepcidin gene increased, which were reversed by ATV. When SMAD7 was knocked down, ATV treatment failed to produce the above effect. ATV also improved ferroptosis in I/R rat myocardium through the SMAD7/hepcidin pathway. **Conclusions.** ATV reversed the decline in H9C2 cell viability, mitochondrial shrinkage, and ROS elevation, and improved the myocardium ferroptosis through the SMAD7/hepcidin pathway in I/R rat.

## 1. Introduction

In recent years, programmed myocardial cell necrosis induced by iron-overload has been found to promote the occurrence of cardiomyopathy [1]. This death does not respond to apoptosis, necrosis, or autophagy inhibitors, but is effectively inhibited by iron-chelating agents, hence, it is named iron-dependent cell death (ferroptosis) [2]. Ferroptosis is characterized by excessive lipid peroxidation of

polyunsaturated fatty acids (PUFAs) in the biofilms, resulting in cell membrane perforation and cell death [3]. Xuexian Fang et al. found that ferroptosis played a key role in doxorubicin-induced cardiomyopathy [4]. Targeting ferroptosis for the prevention and treatment of cardiomyopathy has heralded new prospects.

Atorvastatin (ATV) is a statin that inhibits the enzyme hydroxymethylglutaryl-CoA reductase and works by down-regulating the LDL cholesterol levels [5]. ATV has anti-

inflammatory, antioxidant, fatty acid metabolism and other functions [6, 7]. In clinical practice, ATV was widely used in the treatment of hyperlipidemia, coronary artery disease, and other atherosclerotic diseases [8]. In addition, the protective effect of ATV in I/R cardiomyopathy and diabetic cardiomyopathy has been repeatedly confirmed by several studies [9, 10]. More and more studies have confirmed the regulatory effect of ATV on ferroptosis. However, studies on how ATV affects ferroptosis in cardiomyopathy were incomplete.

Bone Morphogenetic Protein (BMP)-small mothers against decapentaplegic (SMAD) signaling pathway was the core of regulating hepcidin transcription [11]. SMAD7 was an inhibitory SMAD protein that mediated the negative feedback loop of BMP signal transduction to effectively inhibit the expression of hepcidin [12]. Previous studies have found that the BMP-SMAD signal axis in hepatocytes was the core signal mediating the expression and secretion of hepcidin induced by the IL-6 signal [13]. Hepcidin is a hormone that regulates the absorption, storage, and transport of iron throughout the body [14]. Hepcidin deficiency disrupts iron homeostasis leading to the common iron-overload syndrome [15]. These studies suggested that the effect of ATV on the ferroptosis of cardiomyopathy might be realized by regulating SMAD7/hepcidin.

We hypothesized that ATV might inhibit ferroptosis of H9C2 cells by regulating SMAD7/hepcidin expression to improve I/R injury. This study aims to explore the mechanism of ATV in ischemia-reperfusion (I/R) injury through *in vitro* and *in vivo* models, which provide a new treatment strategy for patients with iron-overload cardiomyopathy.

## 2. Materials and Methods

**2.1. Cell Culture and Treatment.** Rat cardiomyocytes H9C2 (CBP60588, Cbioer) cells were maintained in a DMEM medium (D5796, Sigma) supplemented with 10% FBS (10099141, Gibco) and multiplied at 37°C at 5% CO<sub>2</sub>. Penicillin and streptomycin (SV30010, Beyotime) were added to prevent bacterial contamination. The cells were randomly divided into six groups: control, erastin, H/R, ATV, erastin + ATV, and H/R + ATV groups. The cells were treated differently according to groups. The cells erastin and erastin + ATV groups were treated with erastin (5 μM) for 24 h [16]. The steps of cell hypoxia/reoxygenation (H/R) stimulation were as follows: H9C2 cells were exposed to hypoxia (1% O<sub>2</sub>/94% N<sub>2</sub>/5% CO<sub>2</sub>) for 4 h, followed by oxygen for 2 h [17]. The working concentration of ATV was 1 μM, and the incubation time was 24 h [18].

In order to study the mechanism of ATV, the cells were divided into four groups: H/R, H/R + SMAD7i, H/R + ATV, and H/R + SMAD7i + ATV groups. SMAD7i were constructed by transfecting siRNA targeting SMAD7 into H9C2 cells. siRNA targeting rat SMAD7 (5'-AGGCAUCCUCG GAAGUCATT-3') and the negative control (NC) were synthetic by Tsingke Biotechnology Co., Ltd. [19]. Lipofectamine 2000 (12566014, ThermoFisher) reagent diluted with a serum-free medium was used to aid transfection. DMEM containing FBS was replaced 4 h after transfection.

**2.2. Animal Experiment and Grouping.** A total of 18 Wistar rats (250~300 g) were purchased from Hunan slake Jingda experimental animal Co., Ltd. The rats were randomly divided into the Sham group, I/R group, and I/R + ATV group ( $n = 6/\text{group}$ ). They received standard diet and water before myocardial I/R. Rats in the I/R + ATV group were orally treated with ATV (10 mg/kg/d) for 2 weeks before myocardial I/R (9). The Sham and I/R model rats [9, 20] were constructed as follows: The rats were anesthetized with sodium pentobarbital (50 mg/kg, intraperitoneal injection), ligation of the left anterior descending branch with 4-0 silk thread for 30 min, and then reperfusion for 180 min. In the sham control group, the entire procedure was performed with silk thread passing below the coronary artery, but the LAD coronary artery was not ligated. At the end of reperfusion, the rats were given excessive isoflurane for 10 min and sacrificed by bloodletting. Then the rat myocardial tissues were isolated for subsequent detection.

**2.3. Cell Count Kit-8 assay (CCK8).** The cells were decomposed into single cells by trypsin digestion solution (C0201, Beyotime) and inoculated into a 96-well plate (0030730119, Eppendorf) at a density of  $5 \times 10^3$  cells per well. Each group was set with 3 wells. A 100 μL complete culture medium containing CCK8 (NU679, Dojindo) was added to each well. The cells were incubated at 37°C for 4 h at 5% CO<sub>2</sub> [21]. Then the optical density (OD) value at 450 nm was analyzed by an abio-tek microplate (MB-530, HEALES).

**2.4. HE Staining.** Rat myocardium was immobilized in 4% paraformaldehyde for 24 h and then dehydrated in a gradient of 20% and 30% sucrose solution. The myocardial tissues of rats were embedded in paraffin, sequentially sliced, connected to the treated slides, and baked at 60°C for 12 h. The sections were dewaxed to water by xylene and gradient ethanol (75~100%). Hematoxylin and eosin (Wellbio) were used for section staining. The sections were observed with a microscope (BA210T, Motic).

**2.5. Transmission Electron Microscope (TEM).** The cells were fixed with 2.5% glutaraldehyde and 1% osmium. Gradient concentrations of ethanol were used to dehydrate cells. The cells were incubated with 1:1 epoxy propane-epoxy resin and pure epoxy resin for 2 h, respectively. The cells were coated with pure epoxy resin and baked at 40°C for 12 h, followed by 60°C for 48 h. The cells were stained with lead and uranium salts and observed by transmission electron microscopy (JEM1400, Japan Electronics). Images were recorded with a Morada G3 digital camera.

**2.6. Reactive Oxygen Species (ROS) Detection.** ROS kits (S0033S, Beyotime) were used to detect the ROS level in cells. The mother solution of DCFH-DA was diluted with a serum-free medium to obtain 10 μM of DCFH-DA working solution. Then the culture medium was removed. The cells were immersed with DCFH-DA working solution. The cells were placed in a 37°C cell culture chamber and incubated for

20 min. The cells were washed three times with a serum-free cell culture medium to fully remove DCFH-DA that did not enter the cells. The cells were digested into a single-cell suspension using trypsin digestion solution. The fluorescence signal was detected by flow cytometry.

In addition, we used C11-BODIPY fluorescent probe (D3861, thermofisher) to detect the ROS level again. In brief, the mother solution was obtained by adding 396  $\mu$ l of DMSO to 1 mg of fluorescent probe at a concentration of 5 mM. The cells were diluted in the ratio of 1:1000 and stained at 37°C for 30 min in darkness, washed with PBS for three times in darkness, and then tested by flow cytometry.

**2.7. Western Blot.** Total protein was extracted with RIPA lysate (P0013 B, Beyotime) and quantified with a BCA protein quantification kit. SDS-PAGE electrophoresis was performed to separate proteins. The target proteins were then transferred to a cellulose nitrate (NC) membrane. The NC membrane was sealed with skim milk (5%). Then the membrane was incubated with ACSL4 (1:2000, 22401-1-AP, Proteintech), COX2 (1:1000, 66351-1-Ig, Proteintech), CPX4 (1:5000, 67763-1-Ig, Proteintech), SLC7A11 (1:2000, ab175186, Proteintech), SMAD7 (1:1000, 25840-1-AP, Proteintech), FPN1 (1:800, 26601-1-AP, Proteintech), p-SMAD1 (1:2000, 28865-1-AP, Proteintech), Hepcidin (1:3000, ab30760, Abcam), SMAD1 (1:800, 10429-1-AP, Proteintech), and GAPDH (1:5000, 10494-1-AP, Proteintech). Then it was incubated with secondary antibodies HRP goat antimouse IgG (1:5000, AWS0001a, Abiowell) and HRP goat antirabbit IgG (1:6000, AWS0002a, Abiowell) for 90 min, respectively. The protein bands were visualized using SuperECL Plus luminescence solution (K-12045-D50, Advansta). Chemiscope6100 (CLINX) was used to capture images.

**2.8. Enzyme-Linked Immunosorbent Assay (ELISA).** Rat Hecp ELISA Kit (E-EL-R0500c) was purchased from Elabscience Biotechnology Co., Ltd. Iron Assay kit (ab83366) was purchased from Abcam. All steps were carried out in strict accordance with the instructions. After the reaction was terminated, the OD value of each well at 450 nm was detected by a bio-tek microplate (MB-530, HEALES).

**2.9. Quantitative Polymerase Chain Reaction (qPCR).** The trizol was used to extract total RNA from cells and rat myocardial tissues. Primers of target genes (Table 1) were synthesized by Tsingke Biotechnology Co., Ltd. The cDNA was obtained by reverse transcription of mRNA using HiFscript cDNA Synthesis Kit (CW2569, CWBIO). A fluorescent quantitative PCR instrument (PIKOREAL96, Thermo) was used to amplify cDNA and detect the fluorescence signal. GAPDH was used as an internal reference. The relative expression levels of target genes were calculated by the  $2^{-\Delta\Delta C_t}$  method.

**2.10. Statistical Analysis.** GraphPad Prism (8.0.1) was used to analyze data. Data were presented as the mean  $\pm$  standard deviation. Unpaired students' *t*-test was used to compare two groups; one-way analysis of variance (ANOVA) followed by Tukey post hoc test was utilized for multiple groups. A statistical significance was defined at  $P < 0.05$ .

### 3. Results

**3.1. ATV Inhibited the Ferroptosis of H9C2 Cells.** Firstly, we studied the effect of ATV on the ferroptosis of H9C2 cells. Figure 1(a) showed that cell viability decreased in the erastin and H/R groups compared with the control group. Compared with the erastin or H/R groups, cell viability in the erastin + ATV and H/R + ATV groups increased (Figure 1(a)). Compared with the control group, cells in the erastin and H/R groups showed mitochondrial shrinkage, increased membrane density, and decreased mitochondrial crest number, which was characteristic of ferroptosis (Figure 1(b)). After ATV treatment, the volume of mitochondria and the number of mitochondrial cristae increased (Figure 1(b)). Next, we detected ROS in the cells. As shown in Figure 1(c), ATV reversed abnormally elevated ROS levels (DCFH-DA solution and C11-BODIPY fluorescent probe) in the erastin and H/R groups. GPX4 and SLC7A11 levels were lower in the erastin and H/R groups than in the control group, while ACSL4 and COX2 levels were higher in the erastin and H/R groups (Figure 1(d)). ATV treatment reversed this trend (Figure 1(d)). These results showed that ferroptosis in H9C2 cells was successfully induced by erastin and H/R and ATV significantly alleviated it.

**3.2. ATV Regulated Cellular Iron Homeostasis of H9C2 Cells.** We then investigated the effect of ATV on iron homeostasis in H9C2 cells. As shown in Figure 2(a), ATV treatment reduced abnormally elevated concentrations of total iron and  $Fe^{2+}$  in the cell of H/R group. At the same time, the concentration of total iron and  $Fe^{2+}$  in cell supernatant increased (Figure 2(a)). These results suggested that ATV could promote total iron and  $Fe^{2+}$  excretion from H9C2 cells. The expression levels of hepcidin, IRPs, and TFRC1 were significantly decreased, and the expression levels of FTH and FPN1 were increased in the H/R + ATV group than that in the H/R group (Figures 2(b) and 2(c)). All the results proved that ATV promoted iron ion excretion in H9C2 cells at the molecular level.

**3.3. ATV Activated the SMAD7 Expression.** To investigate the molecular mechanism of ATV in the H/R-induced H9C2 cells ferroptosis, we examined the expression of genes and proteins associated with the SMAD7 pathway. Compared with the control group, the expression of the SMAD7 gene in the H/R group decreased, while the expression level of hepcidin increased (Figure 3(a)). After treatment with ATV (the H/R + ATV group), the expression level of the SMAD7 gene increased, while the expression level of hepcidin

TABLE 1: qPCR primer sequences.

Gene	Sequences (5'-3')	Product length (bp)
TFR1	F: GCCACAAGCCAAACAATATCCG R: ACACTGCTCCCATAATGTGA	250
IRP1	F: TATGCGTGGAACCCCAAGTC R: TGTTCCCCGCTGGAGAGATA	157
TFH	F: TGAGCCCTTTGCAACTTCGT R: CTTCAGGGCCACATCATCCC	217
FPN1	F: CAGGCTTAGGGTCTACTGCG R: GAGGAACCGGAGATAGCACG	210
SMAD7	F: GAGTCTCGGAGGAAGAGGCT R: CTGCTCGATAAGCTGCTGG	84
Hamp	F: CAGACGAGACAGACTACGGC R: TCTCGCTTCCTTCGCTTCAG	95
GAPDH	F: ACAGCAACAGGGTGGTGGAC R: TTTGAGGGTGCAGCGAACTT	252

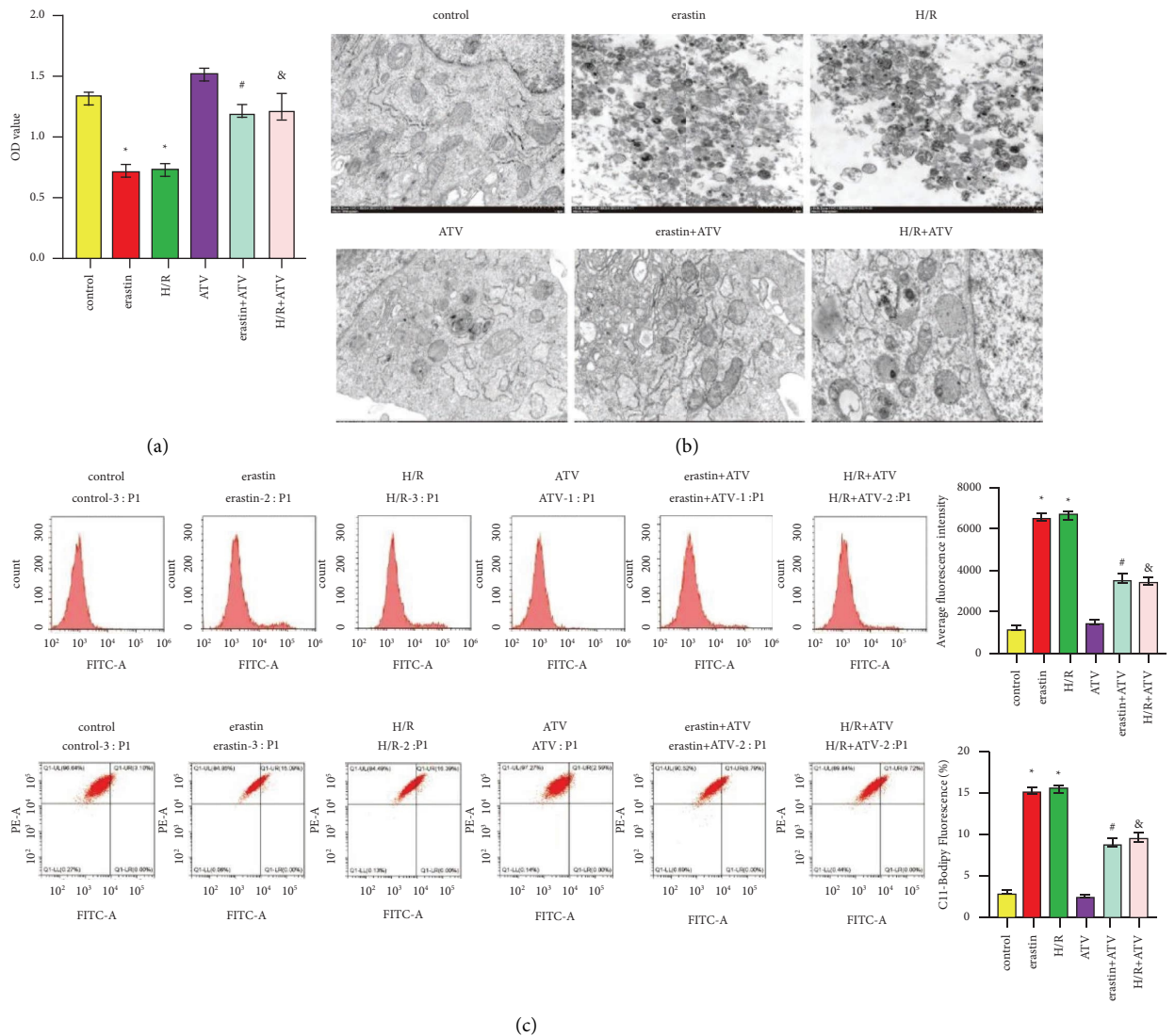


FIGURE 1: Continued.

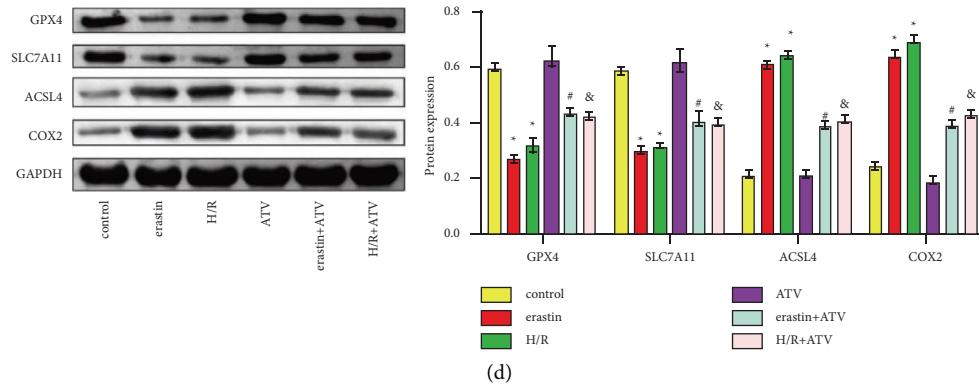


FIGURE 1: ATV inhibited the ferroptosis of H9C2 cells. (a). CCK8 was performed to measure cell vitality. (b). TEM was conducted to observe mitochondrial morphology. Magnification = 10 k and Scale bar = 1.0  $\mu$ m. (c). ROS level was detected by DCFH-DA solution and C11-BODIPY fluorescent probe in H9C2 cells with different treatments. (d). Protein expression was tested by WB. \* $P < 0.05$  vs. the control group. # $P < 0.05$  vs. the erastin group. And  $P < 0.05$  vs. the H/R group.

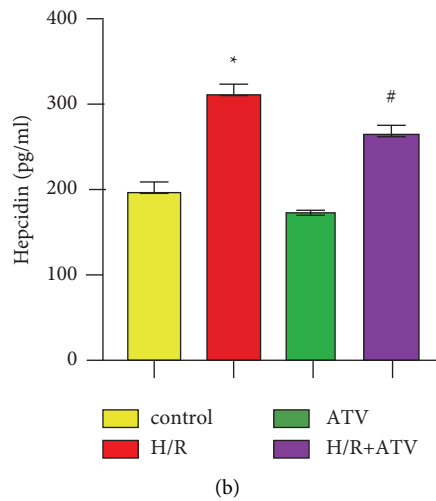
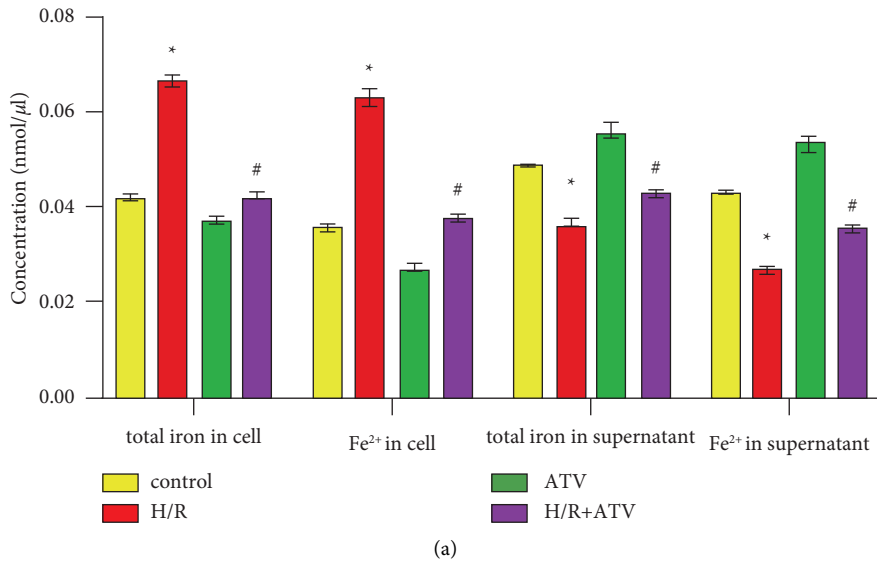


FIGURE 2: Continued.

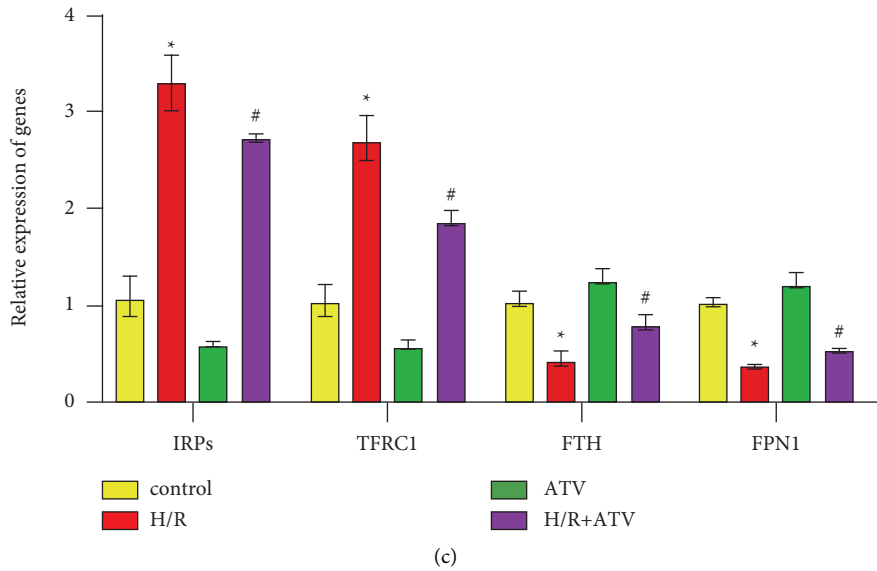


FIGURE 2: ATV regulated cellular iron homeostasis of H9C2 cells. (a-b). The concentration of total iron, Fe<sup>2+</sup>, and hepcidin was calculated by ELISA. (c). The relative expression of genes was measured by qPCR. \*P < 0.05 vs. the control group. #P < 0.05 vs. the H/R group.

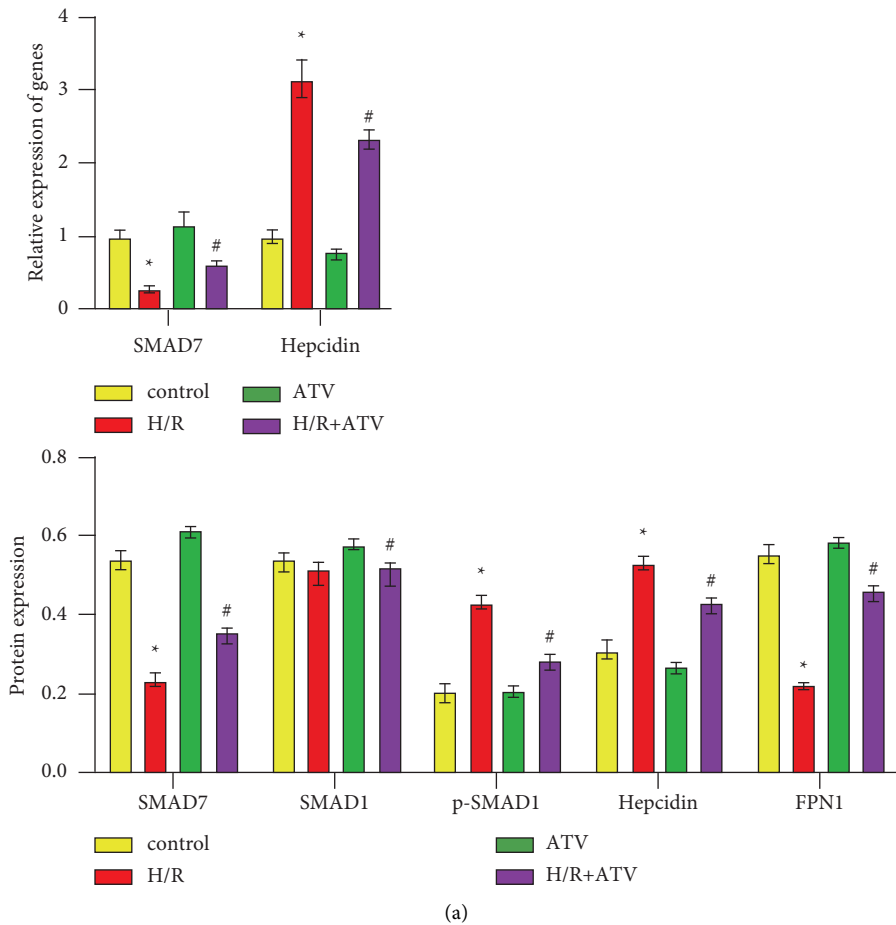


FIGURE 3: Continued.

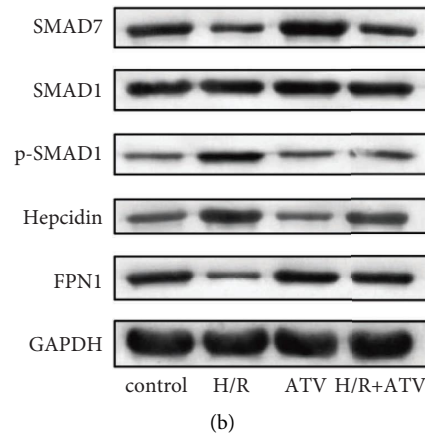


FIGURE 3: ATV activated the SMAD7 expression. (a). The relative expression of SMAD7 and hepcidin was detected by qPCR. (b). WB was used to analyze the proteins expression. \* $P < 0.05$  vs. the control group. # $P < 0.05$  vs. the H/R group.

decreased (Figure 3(a)). At the protein level, compared with the H/R group, the expression of SMAD7 and FPN1 in the H/R+ATV group increased, while the expression of p-SMAD1 and hepcidin decreased (Figure 3(b)). These results indicated that ATV could activate the expression of SMAD7 to regulate the hepcidin/FPN1 pathway.

#### 3.4. ATV Inhibited Ferroptosis in H9C2 Cells through SMAD7.

Then, we knocked down the SMAD7 gene in H9C2 cells. As shown in Figures 4(a) and 4(b), compared with the H/R+SMAD7i group, the gene expression levels of SMAD7, hepcidin, IRPs, TFRC1, FTH, and FPN1 in the H/R+SMAD7i+ATV group showed no significant difference. Figure 4(c) showed that there was no significant difference in the total iron and  $Fe^{2+}$  between H/R+SMAD7i and H/R+SMAD7i+ATV groups. These results reflected that ATV treatment could not regulate iron homeostasis in H9C2 cells in the absence of SMAD7. CCK8 showed that there was no significant difference in cell viability between H/R+SMAD7i and H/R+SMAD7i+ATV groups (Figure 4(d)). These results demonstrated that the inhibition of ferroptosis in H9C2 cells by ATV was realized by regulating SMAD7.

#### 3.5. ATV Resisted Rat Myocardial Ferroptosis by SMAD7/Hepcidin.

HE staining showed that myocardial tissue structure was intact and myocardial cells were arranged neatly in the Sham group (Figure 5(a)). In the I/R group, myocardial tissue cells were disordered, with swelling, necrosis, and myocardial boundary rupture (Figure 5(a)). The myocardial tissues of the I/R+ATV group were better than that of the I/R group (Figure 5(a)). Compared with the Sham group, the contents of  $Fe^{2+}$  and total iron in myocardial tissues of the I/R group were significantly increased (Figure 5(b)). ATV intervention down-regulated the levels of  $Fe^{2+}$  and total iron in I/R rat myocardial tissues (Figure 5(b)). In addition, the expressions of IRPs and TFR1 were increased, and the expressions of FTH and FPN1 were decreased in the I/R group (Figure 5(c)). ATV intervention

inhibited the expression of IRPs and TFR1, and promoted the expression of FTH and FPN1 in I/R rat myocardium (Figure 5(c)). Protein expression analysis showed that compared with the Sham group, the expressions of ASCL4, hepcidin, and p-SMAD1 were increased, and the expressions of GPX4 and SMAD7 were decreased in myocardial tissues of the I/R group (Figures 5(d) and 5(e)). ATV intervention inhibited the expression of ASCL4, hepcidin, and p-SMAD1, and promoted the expression of GPX4 and SMAD7 in I/R rat myocardial tissues (Figures 5(d) and 5(e)). These results suggested that ATV improved ferroptosis in I/R rat myocardium by the SMAD7/hepcidin pathway.

## 4. Discussion

In general, increased iron uptake (e.g., due to TFR overexpression), reduced iron storage (e.g., due to ferritin knockdown or induction of ferritin phagocytosis), and impaired cellular iron output (e.g., due to FPN knockdown) enhanced the sensitivity of cells to ferroptosis [22]. Although in many types of cancer, statins were thought to induce ferroptosis to exert antitumor effects [23]. But in other processes, ATV reduced epidermal growth factor-induced ROS production and up-regulated GPX4 protein expression in rat vascular smooth muscle [24]. Qing Li et al. were the first to demonstrate that fluvastatin protected endothelial cells from ox-LDL-induced ferroptosis and dysfunction [25]. In our study, ATV treatment mitigated erastin or H/R-induced ferroptosis in H9C2 cells. All these studies supported that ATV could block ferroptosis in H/R-induced H9C2 cells injury.

In sepsis-induced acute kidney injury mouse model, ATV (ATV/PTP TCeria NPs) has excellent antioxidant and antiapoptotic activities, which could protect mitochondrial structure and reduce renal injury [26]. In addition, ATV attenuated isoflurane (1.5%) exposure-induced ROS generation and neuronal apoptosis in C57BL/6 mice [27]. ATV could also inhibit the generation of ROS in peripheral blood mononuclear cells of diabetic patients [28]. Our study found ATV reversed abnormally elevated ROS levels (DCFH-DA

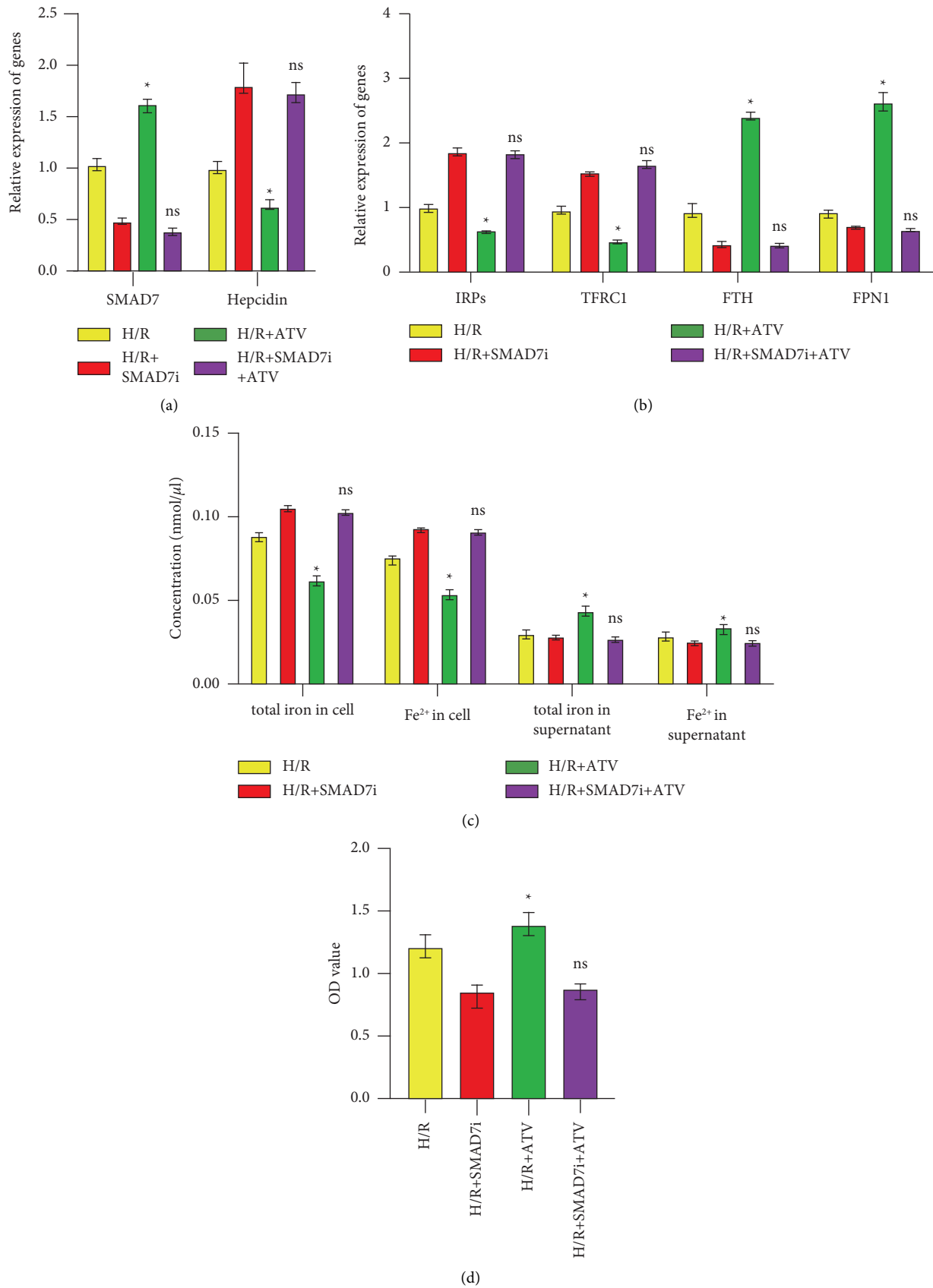


FIGURE 4: ATV inhibited ferroptosis in H9C2 cells through the SMAD7/hepcidin pathway. (a–b).The relative expression of SMAD7, hepcidin, IRPs, TFRC1, FTH, and FPN1 were detected by qPCR. (c). ELISA was utilized to determine the concentration of total iron and Fe<sup>2+</sup>. (d). The cell vitality was measured by CCK8. \*P < 0.05 vs. the H/R group. ns: no significant difference vs. the H/R + SMAD7i group.



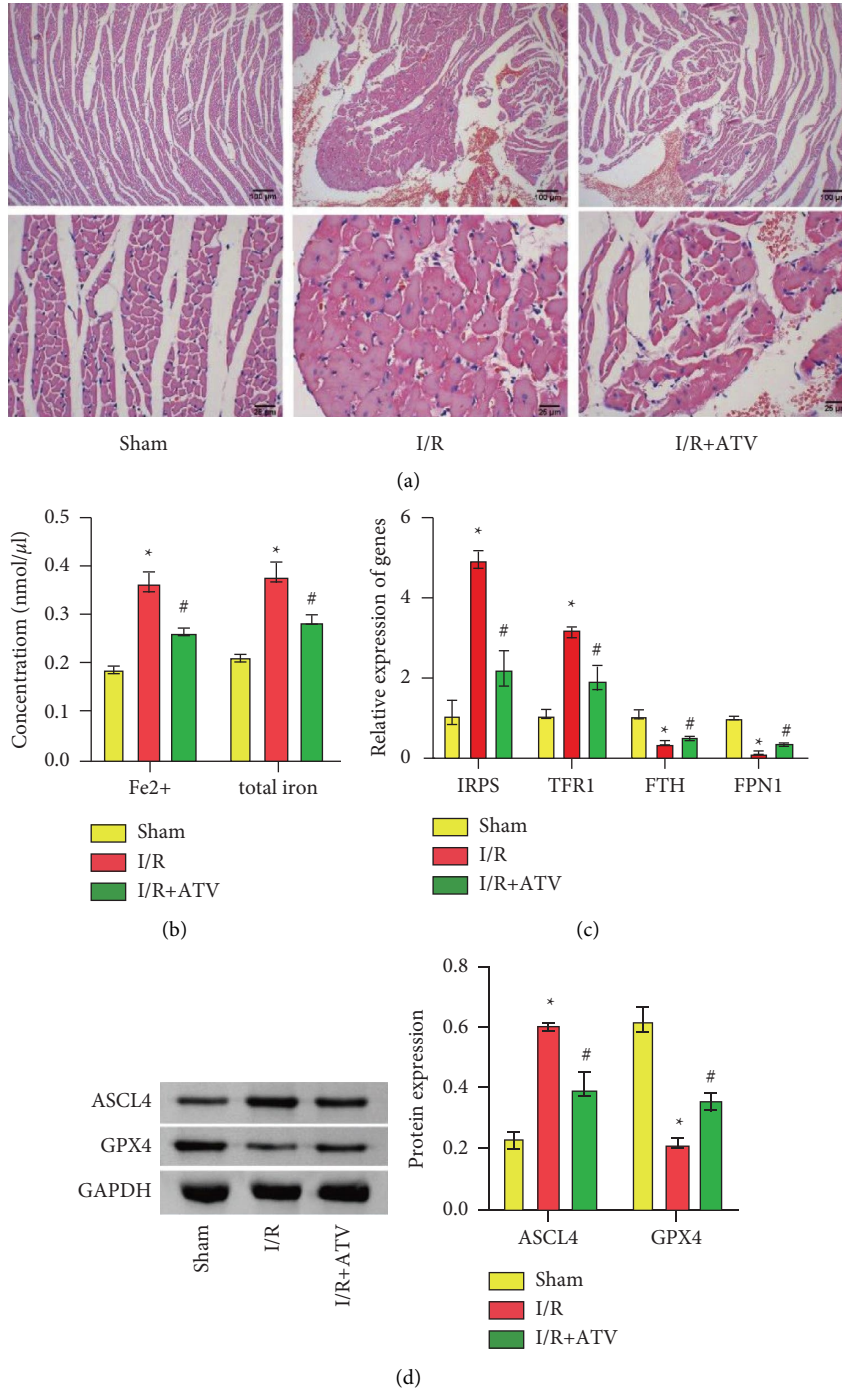


FIGURE 5: Continued.

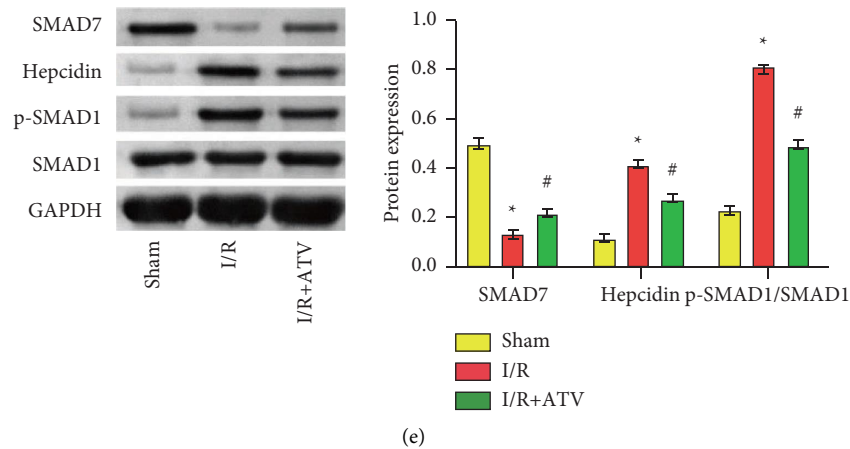


FIGURE 5: ATV improved ferroptosis in I/R rat myocardium by the SMAD7/hepcidin pathway. (a) Cardiac histopathology was observed by HE staining (100 $\times$  and 400 $\times$ ). (b) The levels of Fe<sup>2+</sup> and total iron were detected by ELISA. (c) The expression of IRPs, TFRC1, FTH, and FPN1 was detected by qPCR. (d–e) The expression of ACSL4, GPX4, SMAD7, SMAD1, p-SMAD1, and hepcidin proteins was detected by Western blot. \* $P < 0.05$  vs. the sham group; # $P < 0.05$  vs. the I/R group.

solution and C11-BODIPY fluorescent probe) in the erastin and H/R-induced H9C2 cells. All the studies proved ATV could inhibited ROS generation in H/R-induced H9C2 cells injury.

Ferroptosis was usually accompanied by substantial iron accumulation [29]. Transferrin receptor 1 (TFRC1) and FPN1 controlled iron inflow and outflow, respectively [30]. The stability of the former mRNA was positively regulated by iron regulatory proteins (IRPs), while the latter was negatively regulated by hepcidin [31]. Loss of FTH promoted cardiomyopathy through SLC7A11-mediated ferroptosis [30]. Our study found that ATV regulated intracellular iron homeostasis in erastin or H/R-induced H9C2 cells. All these studies supported that ATV could regulate intracellular iron homeostasis in H/R-induced H9C2 cells injury.

Previously, ATV intervention reduced SMAD7 protein expression in human atrial fibroblasts [32]. Statins inhibited angiotensin II-induced activation of SMAD and associated vascular fibrosis through a TGF- $\beta$  independent process [33]. ATV promoted the antifibrotic effect on the myocardium by inhibiting SMAD2 activity [34]. Statins consume cholesterol to inhibit SMAD1 phosphorylation and nuclear translocation in cultured sensory neurons [35]. Our study found that H/R-induced SMAD7 expression was up-regulated, and phosphorylation of SMAD1 expression was decreased in H9C2 cells after ATV treatment. All these studies demonstrated the activation of SMAD7 by ATV in H/R-induced H9C2 cells and I/R rat myocardium.

In addition, we found that ATV intervention decreased the hepcidin expression and increased the FPN1 expression in H/R-induced H9C2 cells. In a study of patients with stage 3 and 4 chronic kidney disease, 6 months of ATV administration reduced hepcidin expression [6]. The BMP-SMAD pathway was a classic pathway for regulating iron by activating the IL-6/hepcidin signal and reducing serum iron and transferrin saturation [36]. Hepcidin was an important factor leading to iron overload in cerebral ischemia [37]. Knockdown of ferritin inhibited the increase of L-ferritin

and decrease of FPN1 in I/R [38]. Our study proved ATV intervention up-regulated the expression of SMAD7 in H9C2 cells induced by H/R, thereby inhibiting the SMAD pathway and down-regulating the expression of hepcidin, and activating FPN1 to transport intracellular iron out of the cell.

ATV and its two active metabolites *o*-hydroxyatorvastatin (*o*-OH-ATV) and *p*-hydroxyatorvastatin (*p*-OH-ATV) are responsible for its HMG-CoA (3-hydroxy-3-methylglutaryl CoA) reductase inhibitory activity, while the corresponding inactive lactone form (LAC) was associated with myopathy [39]. Our *in vivo* study firstly proved that ATV inhibited ferroptosis in I/R rat myocardium. However, its drug metabolism and stability in rats still need to be further evaluated. It was known that the porous polylactic acid membrane loaded with ATV hot gel has excellent anti-inflammation ability and good anti-adhesion ability [40], which has great potential for clinical application of ATV in I/R myocardium.

H<sub>2</sub>O<sub>2</sub> increased iron concentration in retinal pigment epithelial cells via the BMP6/SMAD/hepcidin axis, resulting in age-related macular degeneration [41]. Inhibitory SMAD7 is a key repressor of hepcidin, the master regulator of systemic iron homeostasis [42]. ATV therapy improves isoprenaline attack-induced cardiac function and remodeling by reducing ferroptosis [43]. ATV reverses barrier dysfunction, oxidative stress, and ferroptosis in human lung microvascular endothelial cells induced by cigarette smoke extract [44]. Our *in vivo* and *in vitro* study proved that ATV inhibited ferroptosis in I/R rat myocardium through the SMAD7/hepcidin pathway, which provides new insights for the clinical application of ATV in I/R myocardium.

## 5. Conclusion

ATV intervention blocked erastin or H/R-induced ferroptosis in H9C2 cells by activating SMAD7 expression and thereby down-regulating the hepcidin/FPN1 pathway. The

*in vivo* study also demonstrated that ATV inhibited ferroptosis in I/R rat myocardium through the SMAD7/hepcidin pathway.

### Data Availability

The data used to support the findings of this study are available from the corresponding author upon request.

### Ethical Approval

This study was approved by the Ethics Committee of the Hunan Provincial People's Hospital. All experimental procedures were conducted in accordance with institutional guidelines for the use of experimental animals.

### Conflicts of Interest

The authors declare that they have no conflicts of interest.

### Authors' Contributions

You Peng and Zhi-Yu Zeng designed the study. You Peng, Bin Liao, Yan Zhou, and Wei Zeng participated in material collection. You Peng and Bin Liao wrote the manuscript. Yan Zhou and Zhi-Yu Zeng revised the manuscript. All authors read and approved the final manuscript.

### Acknowledgments

This study was supported by Hunan Provincial Health Committee Foundation (No. 20200102) and Key Scientific Research Project of Hunan Provincial Department of Education (No. 21A0044) and Guangxi Clinical Research Center for Cardio-Cerebrovascular Diseases (Grant No. AD17129014) and Guangxi Key Laboratory of Precision Medicine in Cardio-Cerebrovascular Diseases Control and Prevention (Grant No. 19-245-34).

### References

- [1] X. Wu, Y. Li, S. Zhang, and X. Zhou, "Ferroptosis as a novel therapeutic target for cardiovascular disease," *Theranostics*, vol. 11, no. 7, pp. 3052–3059, 2021.
- [2] S. J. Dixon, K. M. Lemberg, M. R. Lamprecht et al., "Ferroptosis: an iron-dependent form of nonapoptotic cell death," *Cell*, vol. 149, no. 5, pp. 1060–1072, 2012.
- [3] B. R. Stockwell, X. Jiang, and W. Gu, "Emerging mechanisms and disease relevance of ferroptosis," *Trends in Cell Biology*, vol. 30, no. 6, pp. 478–490, 2020.
- [4] X. Fang, H. Wang, D. Han et al., "Ferroptosis as a target for protection against cardiomyopathy," *Proceedings of the National Academy of Sciences of the U S A*, vol. 116, no. 7, pp. 2672–2680, 2019.
- [5] S. Qiu, W. Zhuo, C. Sun, Z. Su, A. Yan, and L. Shen, "Effects of atorvastatin on chronic subdural hematoma: a systematic review," *Medicine (Baltimore)*, vol. 96, no. 26, Article ID e7290, 2017.
- [6] A. Masajtis-Zagajewska and M. Nowicki, "Effect of atorvastatin on iron metabolism regulation in patients with chronic kidney disease - a randomized double blind crossover study," *Renal Failure*, vol. 40, no. 1, pp. 700–709, 2018.
- [7] G. Gao, S. Jiang, L. Ge et al., "Atorvastatin improves doxorubicin-induced cardiac dysfunction by modulating Hsp70, akt, and MAPK signaling pathways," *Journal of Cardiovascular Pharmacology*, vol. 73, no. 4, pp. 223–231, 2019.
- [8] Y. Xu and Y. Wu, "Atorvastatin associated with gamma glutamyl transpeptidase elevation in a hyperlipidemia patient: a case report and literature review," *Medicine (Baltimore)*, vol. 99, no. 40, Article ID e22572, 2020.
- [9] C. Cheng, X. B. Liu, S. J. Bi, Q. H. Lu, and J. Zhang, "Inhibition of Rho-kinase is involved in the therapeutic effects of atorvastatin in heart ischemia/reperfusion," *Experimental and Therapeutic Medicine*, vol. 20, no. 4, pp. 3147–3153, 2020.
- [10] X. M. Ren, G. F. Zuo, W. Wu et al., "Atorvastatin alleviates experimental diabetic cardiomyopathy by regulating the GSK-3 $\beta$ -PP2Ac-NF- $\kappa$ B signaling Axis," *PLoS One*, vol. 11, no. 11, Article ID e0166740, 2016.
- [11] P. An, H. Wang, Q. Wu et al., "Smad7 deficiency decreases iron and haemoglobin through hepcidin up-regulation by multilayer compensatory mechanisms," *Journal of Cellular and Molecular Medicine*, vol. 22, no. 6, pp. 3035–3044, 2018.
- [12] K. Mleczko-Sanecka, G. Casanovas, A. Ragab et al., "SMAD7 controls iron metabolism as a potent inhibitor of hepcidin expression," *Blood*, vol. 115, no. 13, pp. 2657–2665, 2010.
- [13] C. Besson-Fournier, C. Latour, L. Kautz et al., "Induction of activin B by inflammatory stimuli up-regulates expression of the iron-regulatory peptide hepcidin through Smad1/5/8 signaling," *Blood*, vol. 120, no. 2, pp. 431–439, 2012.
- [14] V. Díaz, E. Gammella, S. Recalcati et al., "Liver iron modulates hepcidin expression during chronically elevated erythropoiesis in mice," *Hepatology*, vol. 58, no. 6, pp. 2122–2132, 2013.
- [15] E. Charlebois and K. Pantopoulos, "Iron overload inhibits BMP/SMAD and IL-6/STAT3 signaling to hepcidin in cultured hepatocytes," *PLoS One*, vol. 16, no. 6, Article ID e0253475, 2021.
- [16] Y. T. Bai, R. Chang, H. Wang, F. J. Xiao, R. L. Ge, and L. S. Wang, "ENPP2 protects cardiomyocytes from erastin-induced ferroptosis," *Biochemical and Biophysical Research Communications*, vol. 499, no. 1, pp. 44–51, 2018.
- [17] Z. Qiu, S. Lei, B. Zhao et al., "NLRP3 inflammasome activation-mediated pyroptosis aggravates myocardial ischemia/reperfusion injury in diabetic rats," *Oxidative Medicine and Cellular Longevity*, vol. 2017, Article ID 9743280, 17 pages, 2017.
- [18] Q. Li and Y. Yang, "AMP-ACTIVATED protein kinase-mediated cardioprotection of atorvastatin relates to the interaction of autophagy and apoptosis in cardiomyocytes exposed to hypoxia/reoxygenation," *Journal of the American College of Cardiology*, vol. 65, no. 10, pp. A153–A, 2015.
- [19] W. Yao, X. Wang, and K. Xiao, "Protective effect of berberine against cardiac ischemia/reperfusion injury by inhibiting apoptosis through the activation of Smad7," *Molecular and Cellular Probes*, vol. 38, pp. 38–44, 2018.
- [20] Z. Li, Y. Li, Z. He, Z. Li, W. Xu, and H. Xiang, "The preventive effect of cardiac sympathetic denervation induced by 6-OHDA on myocardial ischemia-reperfusion injury: the changes of lncRNA/circRNAs-miRNA-mRNA network of the upper thoracic spinal cord in rats," *Oxidative Medicine and Cellular Longevity*, vol. 2021, Article ID 2492286, 28 pages, 2021.
- [21] Y. Hu, H. Zai, W. Jiang, Z. Ou, Y. Yao, and Q. Zhu, "The mutual inhibition of FoxO1 and SREBP-1c regulated the progression of hepatoblastoma by regulating fatty acid metabolism," *Mediators of Inflammation*, vol. 2021, Article ID 5754592, 18 pages, 2021.

- [22] J. Liu, F. Kuang, G. Kroemer, D. J. Klionsky, R. Kang, and D. Tang, "Autophagy-dependent ferroptosis: machinery and regulation," *Cell Chemical Biology*, vol. 27, no. 4, pp. 420–435, 2020.
- [23] X. Chen, R. Kang, G. Kroemer, and D. Tang, "Broadening horizons: the role of ferroptosis in cancer," *Nature Reviews Clinical Oncology*, vol. 18, no. 5, pp. 280–296, 2021.
- [24] S. Wassmann, U. Laufs, K. Müller et al., "Cellular antioxidant effects of atorvastatin in vitro and in vivo," *Arteriosclerosis, Thrombosis, and Vascular Biology*, vol. 22, no. 2, pp. 300–305, 2002.
- [25] Q. Li, C. Liu, L. Deng et al., "Novel function of fluvastatin in attenuating oxidized low-density lipoprotein-induced endothelial cell ferroptosis in a glutathione peroxidase4- and cystine-glutamate antiporter-dependent manner," *Experimental and Therapeutic Medicine*, vol. 22, no. 5, p. 1275, 2021.
- [26] H. Yu, F. Jin, D. Liu et al., "ROS-responsive nano-drug delivery system combining mitochondria-targeting ceria nanoparticles with atorvastatin for acute kidney injury," *Theranostics*, vol. 10, no. 5, pp. 2342–2357, 2020.
- [27] P. Liu, Q. Gao, L. Guan et al., "Atorvastatin attenuates isoflurane-induced activation of ROS-p38MAPK/ATF2 pathway, neuronal degeneration, and cognitive impairment of the aged mice," *Frontiers in Aging Neuroscience*, vol. 12, Article ID 620946, 2020.
- [28] P. M. F. Dos Anjos, C. M. O. Volpe, T. C. Miranda, and J. A. Nogueira-Machado, "Atorvastatin inhibited ROS generation and increased IL-1 $\beta$  and IL-6 release by mononuclear cells from diabetic patients," *Endocrine, Metabolic & Immune Disorders - Drug Targets*, vol. 19, no. 8, pp. 1207–1215, 2019.
- [29] J. Li, F. Cao, H. L. Yin et al., "Ferroptosis: past, present and future," *Cell Death & Disease*, vol. 11, no. 2, p. 88, 2020.
- [30] X. Fang, Z. Cai, H. Wang et al., "Loss of cardiac ferritin H facilitates cardiomyopathy via slc7a11-mediated ferroptosis," *Circulation Research*, vol. 127, no. 4, pp. 486–501, 2020.
- [31] S. Haddad, Y. Wang, B. Galy et al., "Iron-regulatory proteins secure iron availability in cardiomyocytes to prevent heart failure," *European Heart Journal*, vol. 38, no. 5, pp. 362–372, 2017.
- [32] X. Cheng, Q. Huang, and J. Zhang, "Effects of transforming growth factor- $\beta$ 1 and atorvastatin on the expression of collagen type I P-smads in human atrial fibroblasts," *Chinese Circulation Journal*, no. 6, pp. 562–566, 2015.
- [33] R. Rodrigues Díez, R. Rodrigues-Díez, C. Lavoz et al., "Statins inhibit angiotensin II/Smad pathway and related vascular fibrosis, by a TGF- $\beta$ -independent process," *PLoS One*, vol. 5, no. 11, Article ID e14145, 2010.
- [34] B. Yu, M. Yu, H. Zhang, D. Xie, W. Nie, and K. Shi, "Suppression of miR-143-3p contributes to the anti-fibrosis effect of atorvastatin on myocardial tissues via the modulation of Smad2 activity," *Experimental and Molecular Pathology*, vol. 112, Article ID 104346, 2020.
- [35] R. C. Bucelli, E. A. Gonsiorek, W.-Y. Kim et al., "Statins decrease expression of the proinflammatory neuropeptides calcitonin gene-related peptide and substance P in sensory neurons," *Journal of Pharmacology and Experimental Therapeutics*, vol. 324, no. 3, pp. 1172–1180, 2008.
- [36] L. Yang, H. Wang, X. Yang et al., "Auranofin mitigates systemic iron overload and induces ferroptosis via distinct mechanisms," *Signal Transduction and Targeted Therapy*, vol. 5, no. 1, p. 138, 2020.
- [37] P. Wang, Y. Cui, Q. Ren et al., "Mitochondrial ferritin attenuates cerebral ischaemia/reperfusion injury by inhibiting ferroptosis," *Cell Death & Disease*, vol. 12, no. 5, p. 447, 2021.
- [38] H. Ding, C.-Z. Yan, H. Shi et al., "Hepcidin is involved in iron regulation in the ischemic brain," *PLoS One*, vol. 6, no. 9, Article ID e25324, 2011.
- [39] R. N. Cestari, A. Rocha, M. P. Marques, R. D. R. de Oliveira, and V. L. Lanchote, "Simultaneous analysis of the total plasma concentration of atorvastatin and its five metabolites and the unbound plasma concentration of atorvastatin: application in a clinical pharmacokinetic study of single oral dose," *Journal of Chromatography B*, vol. 1126–1127, Article ID 121766, 2019.
- [40] J. Li, X. Feng, J. Shi, T. Liu, and J. Ding, "Porous polylactide film Plus atorvastatin-loaded thermogel as an efficient device for peritoneal adhesion prevention," *ACS Omega*, vol. 3, no. 3, pp. 2715–2723, 2018.
- [41] L. Chen, B. Ma, X. Liu, Y. Hao, X. Yang, and M. Liu, "H<sub>2</sub>O<sub>2</sub> induces oxidative stress damage through the BMP-6/SMAD/hepcidin axis," *Development Growth and Differentiation*, vol. 62, no. 2, pp. 139–146, 2020.
- [42] M. Vujić Spasić, R. Sparla, K. Mleczko-Sanecka et al., "Smad6 and Smad7 are co-regulated with hepcidin in mouse models of iron overload," *Biochimica et Biophysica Acta - Molecular Basis of Disease*, vol. 1832, no. 1, pp. 76–84, 2013.
- [43] D. Ning, X. Yang, T. Wang, Q. Jiang, J. Yu, and D. Wang, "Atorvastatin treatment ameliorates cardiac function and remodeling induced by isoproterenol attack through mitigation of ferroptosis," *Biochemical and Biophysical Research Communications*, vol. 574, pp. 39–47, 2021.
- [44] Y. Wang, X. Kuang, Y. Yin et al., "Tongxinluo prevents chronic obstructive pulmonary disease complicated with atherosclerosis by inhibiting ferroptosis and protecting against pulmonary microvascular barrier dysfunction," *Biomedicine & Pharmacotherapy*, vol. 145, Article ID 112367, 2022.